



4th generation nonsteroidal aromatase inhibitors: An iterative SAR-guided design, synthesis, and biological evaluation towards picomolar dual binding inhibitors

Ahmed G. Eissa^{a,1}, Denise Barrow^a, Julia Gee^a, Lauren E. Powell^b, Paul A. Foster^{b,c}, Claire Simons^{a,*}

^a School of Pharmacy and Pharmaceutical Sciences, Cardiff University, King Edward VII Avenue, Cardiff, CF10 3NB, UK

^b Institute of Metabolism and Systems Research, College of Medical and Dental Sciences, University of Birmingham, Birmingham, B15 2TT, UK

^c Centre for Endocrinology, Diabetes, and Metabolism, Birmingham Health Partners, Birmingham, B15 2TT, UK

ABSTRACT

One in every eight women will be diagnosed with breast cancer during their lifetime and approximately 70% of all patients are oestrogen receptor (ER) positive depending upon oestrogen for their growth accounting for third generation aromatase (CYP19A1) inhibitors being the mainstay in the treatment of ER-positive breast cancer. Despite the success of current aromatase inhibitors, acquired resistance occurs after prolonged therapy. Although the precise mechanisms of resistance are not known, lack of cross resistance among aromatase inhibitors drives the need for a newer generation of inhibitors to overcome this resistance alongside minimising toxicity and adverse effects. Novel triazole-based inhibitors were designed based on previously published parent compound **5a**, making use of the now available crystal structure of CYP19A1 (PDB 3S79), to make modifications at specific sites to explore the potential of dual binding at both the active site and the access channel. Modifications included adding long chain substituents e.g. but-2-ynyloxy and pent-2-ynyloxy at different positions including the most active compound **13h** with IC₅₀ value in the low picomolar range (0.09 nM). Aromatase inhibition results paired with molecular dynamics studies provided a clear structure activity relationship and favourable dual binding mode was verified. Toxicity assays and CYP selectivity profile studies for some example compounds were performed to assess the safety profile of the prepared inhibitors providing the basis for the 4th generation nonsteroidal aromatase inhibitors.

1. Introduction

Breast cancer is a complex collection of heterogeneous neoplastic, often recurrent, diseases affecting 1 in 8 women [1–4]. The number of women diagnosed with breast cancer has risen from 1.68 million to 2.1 million between 2012 and 2018 ranking first place of highest incidence malignancies among women with 24% and only second to lung cancer among all populations [3–5]. Different subclasses of breast cancer are responsible of 14.3% of all female cancer related deaths [5,6], approximately 70% of which show dependence on oestrogen/ER signaling for their growth, thus called ER positive [7].

As early as the 1890s, hormonal targeted therapy gained a crucial role over the years in oestrogen deprivation and control of breast cancer [8,9]. ER- α is often directly involved in tumour growth providing the basis for two different classes of antihormonal therapy; interference with binding of oestrogen to the receptor, which is divided into selective oestrogen receptor modulators (SERMs) that are competitive inhibitors of the ER e.g. tamoxifen, and selective oestrogen receptor degraders

(SERDs) e.g. fulvestrant (Fig. 1) [10]. The second strategy is oestrogen deprivation via inhibition of aromatase (CYP19A1) responsible for oestrogen synthesis e.g. anastrozole, letrozole and exemestane (Fig. 1) [9,10]. Despite the success, high efficacy and selectivity of the currently available third generation aromatase inhibitors (AIs), acquired resistance eventually occurs after prolonged therapy along with some cross-activity to other cytochrome P450 (CYP) family members (e.g. anastrozole's inhibition of CYP1A2, letrozole's inhibition of CYP2A6) and some androgenic and/or weak ER α agonistic activity [11–13]. Considerable efforts have been made to date in relation to designing further compounds, some with improved IC₅₀ values compared with the clinically-approved reference compounds and so with promising AI activity. This is the case either for steroidal or nonsteroidal AIs especially after the crystal structure of aromatase (PDB 3EQM) was published [14]. Therefore the design and synthesis of a new generation of inhibitors is needed to widen the therapeutic options available owing to the risk of resistance towards available drugs, and also to minimise toxicity and reduce the non-specific and adverse effects by increasing aromatase

* Corresponding author.

E-mail address: simonsc@cardiff.ac.uk (C. Simons).

¹ Present Addresses: Ahmed G. Eissa, Department of Medicinal Chemistry, Faculty of Pharmacy, Zagazig University, Zagazig P.C. 44519, Egypt.

selectivity [7,11,15]. This led to a continuous exploration of alternative strategies with allosteric inhibition rising as a possibility especially after letrozole and one of the metabolites of tamoxifen; namely endoxifen, were reported to have the potential of non-competitive/mixed inhibition for aromatase [16,17]. This type of inhibition indicates the presence and identification of allosteric sites in aromatase. Three potential allosteric sites were identified through computational studies including the haem proximal site along with two access channels connected to the active site [18–20]. The front door access channel gated by Asp309 was identified in the crystal structure published in 2009 (PDB 3EQM) [14]. On the other side of the active site, a backdoor channel gated with Ser314 was discovered through the crystal structures published in 2018 (PDB 5JKV, 5JKW, 5JL6, 5JL7 and 5JL9), which is postulated to be involved in the passage of catalytic water [14,21].

Allosteric non-competitive inhibition of aromatase offers major advantages over conventional inhibitors in terms of reaching maximum inhibition without the complete blockage of oestrogen production, which would reduce side effects and delay or avoid the onset of resistance along with better selectivity owing to allosteric sites being less conserved across other enzymes. Also, they are not outcompeted by high concentrations of androgens as natural substrate, making this approach appealing for rational drug discovery [18]. Even though there are no reported effective allosteric inhibitors of aromatase, some novel steroidal compounds with a dual-binding ability for the access channel and the active site were reported in 2012 [22].

These potent inhibitors were characterised by a long alkyne side chain at C6 of the steroidal scaffold that could fit through the narrow hydrophobic access channel, which is the main transport route for steroids, water molecules and proton sources, giving rise to the concept of 4th generation steroidal aromatase inhibitors with dual binding capacity (Fig. 2A). The alkyne side chains are proposed to sit in the access channel preventing entry of other molecules and to displace water molecules believed to act catalytically, by proton relay through the Arg192-Glu483 salt bridge pair at the channel entrance and Asp309 within the channel, in the enolization of androstenedione [22]. This is extendable to the non-steroidal AI class as some nonsteroidal xanthone compounds with the same pent-2-yne arm (Fig. 2B) were reported to have aromatase inhibitory activity in low micromolar range in 2020 and

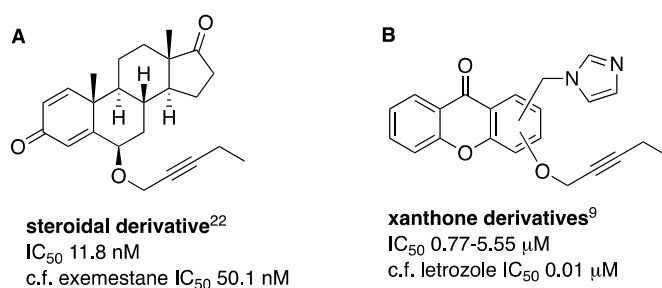


Fig. 2. Reported (A) steroidal and (B) xanthone O-pent-2-yne derivatives with aromatase dual binding capacity.

so this concept is gaining more popularity and may present the molecular basis for the design of 4th generation non-steroidal AIs [9,18,22].

As an early part of this project, 1-[(6-methoxybenzofuran-2-yl)phenylmethyl]triazoles (Fig. 3, R_1 = H, R_2 = OCH₃, R_3 = varying functional groups) were previously reported as potent aromatase inhibitors, presenting a suitable scaffold for incorporation of the hydrophobic tail required for filling the access channel in a dual orthosteric/allosteric inhibition [23]. In this paper, three main variants were studied, the first of which was the position of the hydrophobic tail (Fig. 3, R_1 , R_2 or R_3) to provide an answer to the preferable binding mode. Then the length of the hydrophobic tail was investigated as it was not guaranteed that a five-carbon chain length would be the optimal length for activity in a non-steroidal compound. Along with the nature of the secondary substitution, a more comprehensive SAR was developed with toxicity assessment and CYP selectivity of the compounds with promising aromatase inhibitory activity. These questions were addressed through an iterative process of a design/synthesis/inhibitory evaluation cycle to guide the rational drug design in three distinct comparisons (Fig. 3).

2. Results and discussion

2.1. Chemistry

The synthetic pathways for the previously reported parent AIs (5) and the newly synthesized modified compounds (6 and 7) are outlined

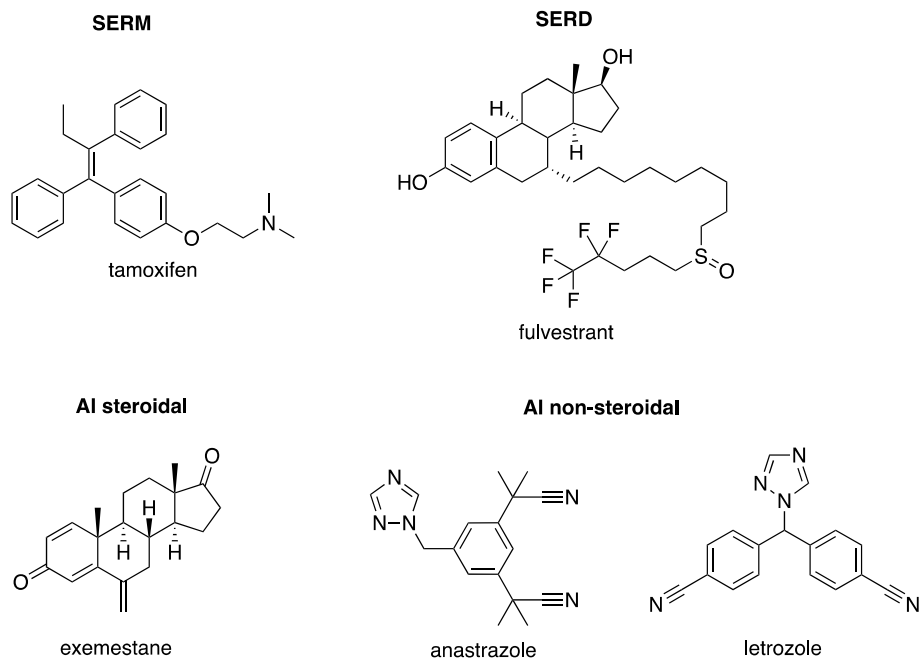


Fig. 1. Clinically used selective oestrogen receptor modulators (SERMs, e.g. tamoxifen), selective oestrogen receptor degraders (SERDs e.g. fulvestrant) and aromatase inhibitors (AIs, e.g. steroidal exemestane, non-steroidal anastrozole and letrozole).

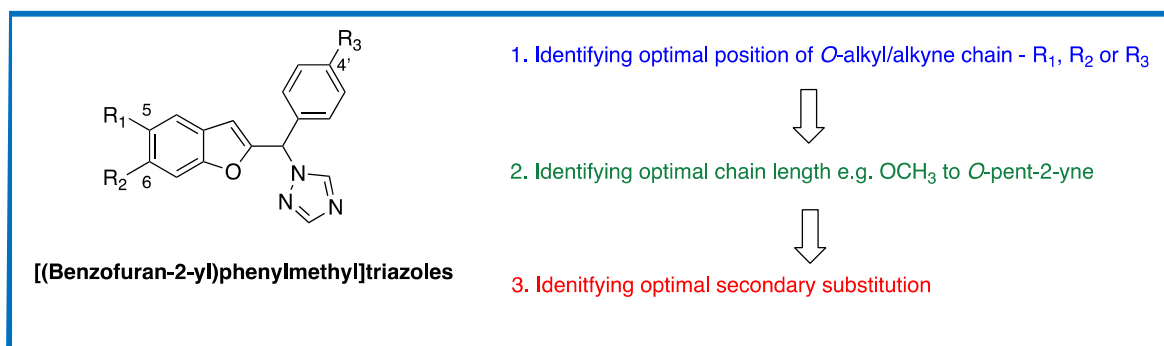


Fig. 3. Proposed process of identifying optimal non-steroidal [(benzofuran-2-yl)phenylmethyl]triazole derivatives as aromatase dual binding site inhibitors.

in Scheme 1. Initially, the parent methoxy substituted compounds were prepared using the reported synthetic pathway as indicated in Scheme 1 with modifications to the methods made where necessary to optimize the reactions [23].

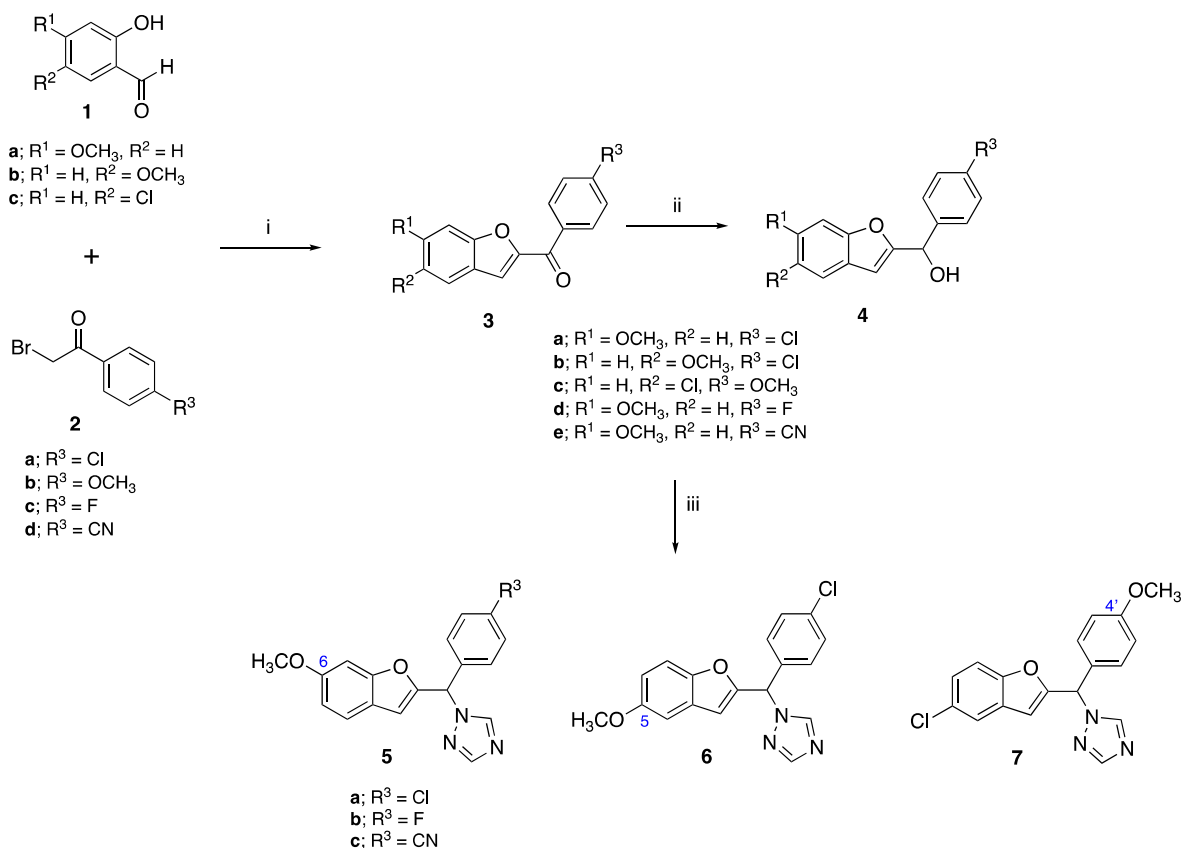
The Rap-Stoermer formation of the benzofurans was performed using the original method with NaH as the base, however it was replaced by K_2CO_3 as reported by Mahboobi et al., to improve the yield (80–96%) [24]. Also, the equivalents of $SOCl_2$ in the third step were increased from equimolar to 1.6 equivalents to optimize the method by reducing the reaction time from 4 days to only 16 h with yields ranging from 31 to 63%.

The new molecules with extended substitutions on the benzofuran ring, ranging from ethoxy to pent-2-ynoxy, were prepared via a divergent pathway (Scheme 2) starting with the hydroxy salicylaldehyde derivative after being pyran protected (8) [23,25]. Following the methods described in Scheme 1, the ketones (9) were obtained in good

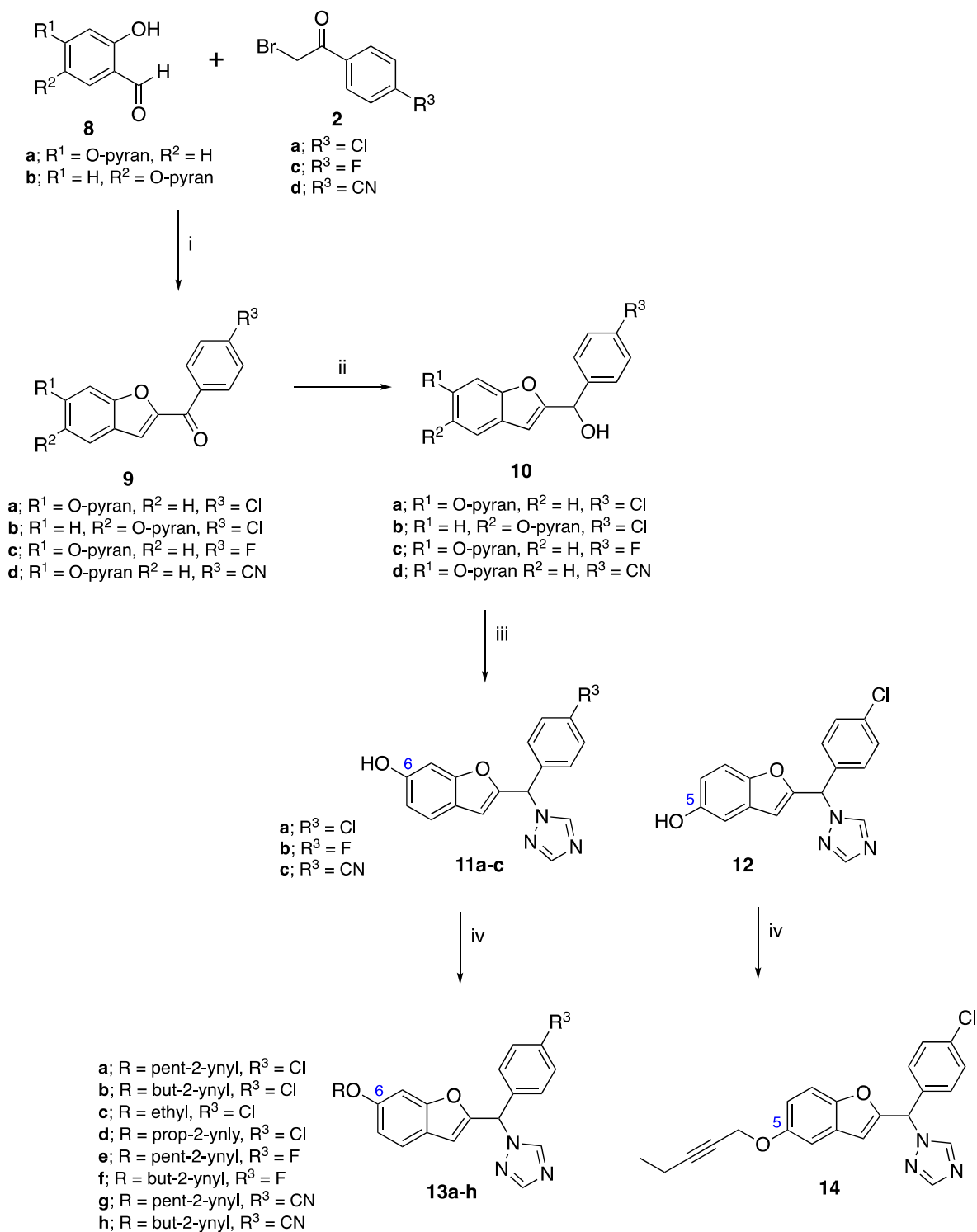
yields (52–95%) and the alcohols (10) obtained in quantitative yield. The introduction of the triazole proceeded with loss of the pyran protection to give the triazole phenol compounds (11 and 12, 44–86%). A final nucleophilic substitution step was required at the end of the synthetic pathway to add the longer alkyloxy chains through Williamson ether synthesis to give the 6-O-alkyl/alkyne (13) and 5-O-pent-2-ynoxy (14) derivatives. The fluoro and chloro derivatives were obtained in good yields (50–90%), however the nitrile derivatives (13g and 13h) were obtained in low yields (7 and 17% respectively) owing to complex reaction mixtures.

The 4'-pent-2-ynoxy compound (19) with the extended substitution on the phenyl side of the compound required a slightly modified pathway (Scheme 3) with the first step being a demethylation of 3c to form 15, which was then pyran protected (16) and proceeded as described in Scheme 2 from the reduction step (17).

The final triazole products were confirmed by 1H and ^{13}C NMR with



Scheme 1. Synthesis of methoxy substituted compounds (5, 6 and 7). *Reagents and conditions:* (i) K_2CO_3 , CH_3CN , $70^\circ C$, 3 h, 80–96%; (ii) $NaBH_4$, dioxane, rt, 2 h, quantitative; (iii) $SOCl_2$, triazole, CH_3CN , $0^\circ C$, 1 h, then 4, CH_3CN , K_2CO_3 , rt, 16 h, 31–63%.

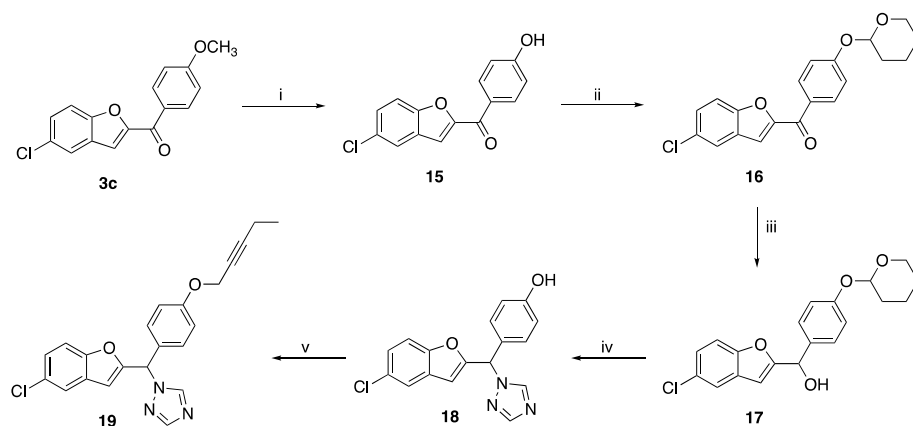


Scheme 2. Synthesis of the 6- and 5-hydroxy and extended compounds (**12–15**). *Reagents and conditions:* (i) K₂CO₃, CH₃CN, 70 °C, 3 h, 52–95%; (ii) NaBH₄, dioxane, rt, 2 h, quantitative; (iii) SOCl₂, triazole, CH₃CN, 0 °C, 1 h, then **10**, CH₃CN, K₂CO₃, rt, 16 h, 44–86%; (iv) K₂CO₃, CH₃CN, 40 °C, 1h, then alkyl bromide, rt, 16 h, 7–90%.

purity determined by HPLC with all compounds $\geq 95\%$ pure. The two characteristic singlets of the triazole group were observed at ~ 8.2 and 8.0 ppm in ^1H NMR and the CH-triazole as either a singlet or finely split triplet ($J = 0.9$ Hz) at ~ 6.5 ppm in ^1H NMR and at ~ 61.5 ppm in ^{13}C NMR.

2.2. Aromatase inhibition

Aromatase activity was assayed using a modified titrated water assay previously reported [26]. Briefly, placental choriocarcinoma JEG-3 cells, known to have high aromatase activity, were grown to approximately 80% confluence in six-well culture plates. Once established, cells were treated with androst-4-ene-3,17-dione [1β - ^3H] as aromatase substrate. Aromatase activity was measured in the absence and presence of



Scheme 3. Synthesis of the 4'-hydroxy and pent-2-ynyloxy derivatives (**18** and **19**). *Reagents and conditions:* (i) HBr, CH₃COOH, 110 °C, 16 h, 57%; (ii) 3,4-dihydro-2H-pyran, *p*-toluenesulfonic acid, EtOAc, rt, 18 h 73%; (iii) NaBH₄, dioxane, rt, 2 h, quantitative; (iv) SOCl₂, triazole, CH₃CN, 0 °C, 1 h, then **17**, CH₃CN, K₂CO₃, rt, 16 h, 45%; (v) K₂CO₃, CH₃CN, 40 °C, 1 h, then 1-bromopent-2-yne, rt, 16 h, 44%.

Table 1

Comparison of 6-, 5- and 4'-hydroxy, methoxy and pent-2-ynyloxy substitution.

Compound	R	CYP19A1 IC ₅₀ (nM)	95% Confidence interval (nM)
6-substitution			
11a	H	0.79	0.724–0.857
5a	CH ₃	0.47	0.449–0.494
13a	CH ₂ C≡CCH ₂ CH ₃	2.76	2.296–3.314
5-substitution			
12	H	5.67	4.965–6.468
6	CH ₃	2.01	1.646–2.452
14	CH ₂ C≡CCH ₂ CH ₃	21.05	16.35–27.11
4'-substitution			
18	H	30.25	25.52–35.86
7	CH ₃	>1000	–
19	CH ₂ C≡CCH ₂ CH ₃	>1000	–
Letrozole		0.70	0.556–0.883

Table 2

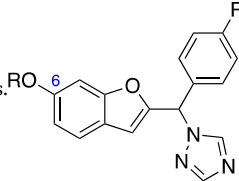
Comparison of the chain length at the optimal 6-position.

Compound	R	CYP19A1 IC ₅₀ (nM)	95% Confidence interval (nM)
5a	CH ₃	0.47	0.449–0.494
13c	CH ₂ CH ₃	0.46	0.378–0.562
13d	CH ₂ C≡CH	1.03	0.674–1.573
13b	CH ₂ C≡CCH ₃	0.53	0.479–0.589
13a	CH ₂ C≡CCH ₂ CH ₃	2.79	2.296–3.314
Letrozole		0.70	0.556–0.883

inhibitors (0.001pM–100pM). Aromatase activity results were determined as a concentration of product formed per mg of protein per hour. Each data point was measured in triplicates and the error in the IC₅₀ calculations represented as 95% confidence interval.

The aromatase inhibitory activity of the 6-, 5- and 4'-hydroxy, methoxy and pent-2-ynyloxy derivatives, with the secondary chloro substituent were first evaluated to determine the effect of the position of

the hydroxy/methoxy/pent-2-ynyloxy groups and the chain length on aromatase inhibition (Table 1). The 6-substituted hydroxy (**11a**), methoxy (**5a**) and pent-2-ynyloxy (**13a**) derivatives showed optimal aromatase inhibition (IC₅₀ 0.79, 0.47 and 2.76 nM respectively) with a reduction in activity observed for the 5-substituted hydroxy (**12**), methoxy (**6**) and pent-2-ynyloxy (**14**) (IC₅₀ 5.67, 2.01 and 21.05 nM respectively). A significant reduction was observed for the 4'-substituted

Table 3Comparison of secondary substitution (R^3) of 6-hydroxy, 6-methoxy, 6-butynyloxy and 6-pentynyloxy derivatives.


Compound	R	R^3	CYP19A1 IC_{50} (nM)	95% Confidence interval (nM)
<i>Cl substitution</i>				
11a	H	Cl	0.79	0.724–0.857
5a	CH ₃	Cl	0.47	0.449–0.494
13b	CH ₂ C≡CCH ₃	Cl	0.53	0.479–0.589
13a	CH ₂ C≡CCH ₂ CH ₃	Cl	2.76	2.296–3.314
<i>F substitution</i>				
11b	H	F	0.39	0.359–0.431
5b	CH ₃	F	0.15	0.101–0.215
13f	CH ₂ C≡CCH ₃	F	4.1	3.283–5.270
13e	CH ₂ C≡CCH ₂ CH ₃	F	0.51	0.419–0.619
<i>CN substitution</i>				
11c	H	CN	0.56	0.504–0.612
5c	CH ₃	CN	0.11	0.092–0.126
13h	CH ₂ C≡CCH ₃	CN	0.09	0.078–0.126
13g	CH ₂ C≡CCH ₂ CH ₃	CN	0.72	0.677–0.759
Letrozole			0.70	0.556–0.883

hydroxy (**18**), methoxy (**7**) and pent-2-ynylkoxy (**19**) (IC_{50} 30.25 nM, > 1 μ M and > 1 μ M respectively), which would indicate the 4'-position to be unfavourable for binding and orientation within the aromatase binding sites.

Having established that the 6-position was optimal, a broader range of chain lengths at the 6-position of the benzofuran ring was investigated (Table 2). The methoxy (**5a**, IC_{50} 0.47 nM), ethoxy (**13c**, IC_{50} 0.46 nM) and but-2-ynyloxy (**13b**, IC_{50} 0.53 nM) were optimal with good aromatase inhibition also observed for the propynyloxy (**13d**, IC_{50} 1.03 nM) compared with the pentynyloxy (**13a**, IC_{50} 2.79 nM), however for binding in both haem binding site and access channel the longer alkyloxy substitutions were preferred.

The effect of the secondary substitution, i.e. substitution of the phenyl ring, on the 6-but-2-ynyloxy and 6-pent-2-ynyloxy derivatives was then evaluated. The choice of secondary substituents, Cl, F and CN, was determined from our previous published research [23] as the most promising substitutions for aromatase inhibition.

For the chloro and nitrile secondary substitutions, the but-2-ynyloxy derivatives (**13b** and **13h** respectively) performed best with low picomolar inhibitory activity observed for the nitrile derivative (**13h**, IC_{50} 0.09 nM), while for the fluoro secondary substitution, the pent-2-ynyloxy derivative (**13e**, IC_{50} 0.51 nM) was optimal (Table 3).

2.3. Toxicity (BrdU) assays

Examples of the compounds, namely **5b**, **11b**, **13e**, and **13h**, were tested at 1 μ M over 48 h along with doxorubicin (Dox) as positive control by bromodeoxyuridine (BrdU) proliferation assay to evaluate the toxicity against non-cancerous breast epithelial cells (MCF-10A) and non-oestrogen dependent breast cancer cells (MDA-MB-231). Statistics using one-way ANOVA followed by a Tukey's Multiple Comparison test comparing all compounds against control showed no significant difference between the tested compounds and the negative control indicating that the compounds had no impact on MCF-10A or MDA-MB-231 growth (Fig. 4). These results suggest possible limited toxicity in normal breast tissue and little off-target effects.

2.4. CYP panel and selectivity

The two lead compounds, 1-((4-fluorophenyl)(6-(pent-2-yn-1-yloxy)benzofuran-2-yl)methyl)-1H-1,2,4-triazole (**13e**) and 4-((6-(but-2-yn-1-yloxy)benzofuran-2-yl)(1H-1,2,4-triazol-1-yl)methyl)benzonitrile (**13h**), were tested for inhibitory activity against a CYP panel (1A2, 2C9, 2C19, 2D6 and 3A4) by Cypotex Discovery Limited using a human liver microsomal assay with a CYP isoform specific probe substrate [27]. The lead fluoro pent-2-ynyloxy lead compound (**13e**) displayed excellent selectivity for CYP19A1 compared with CYPs 3A4 and 2D6 (>277,000 and 49,000 respectively) and very good selectivity compared with CYPs 1A2, 2C9 and 2C19 (10,000, 18,000 and 10,000 respectively) (Table 4). Likewise, the nitrile but-2-ynyloxy lead compound (**13h**) showed excellent selectivity for CYP19A1 compared with CYPs 3A4, 2C9 and 2D6 (>277,000) and very good selectivity compared with CYPs 1A2 and 2C19 (32,000 and 24,000 respectively) (Table 4).

Table 4
CYP IC_{50} (μ M) profile of lead compounds **13h** and **13e**.

Compound	1A2	2C9	2C19	2D6	3A4	19A1
13e	5.3 \pm 0.33	9.2 \pm 1.87	5.21 \pm 0.88	>25	21 \pm 4.82	0.00051
13h	2.88 \pm 0.16	>25	2.17 \pm 0.18	>25	>25	0.00009

Control standards: CYP1A2 α -naphthoflavone IC_{50} 0.02 \pm 0.002 μ M, CYP2C9 sulfaphenazole IC_{50} 0.245 \pm 0.05 μ M, CYP2C19 tranlylcypromine IC_{50} 14.4 \pm 1.62 μ M, CYP2D6 quinidine IC_{50} 0.137 \pm 0.015 μ M, CYP3A4 ketoconazole IC_{50} 0.076 \pm 0.002 μ M.

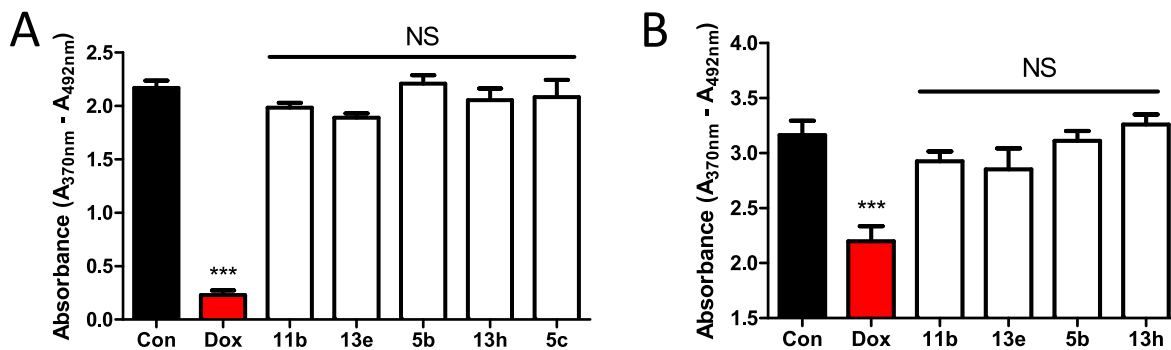


Fig. 4. Toxicity of final compounds tested at 1 μ M for 48 h treatment followed by BrdU proliferation assay in A) MCF-10A and B) MDA-MB-231 cells. Stats are one-way ANOVA followed by a Tukey's Multiple Comparison test comparing all compounds against control (Con) and doxorubicin (Dox, 1 μ M). Data represents n = 5–6 technical replicates \pm SEM. ***p < 0.001 compared to control. NS – Non-significant compared with control.

2.5. Computational studies

Using the crystal structure of human placental aromatase (CYP19A1) refined at 2.75 Å (PDB 3S79) [21], the compounds (*R*- and *S*-enantiomers) were docked using molecular operating environment software (MOE) [28], and the best poses were selected based upon the 3D visual inspection and the score value of the ligand-protein complex (Table S1), which were all subjected to 150 ns MD simulations with longer 400 ns

simulations run for exemplar compounds, using the Desmond programme of Schrödinger software [29,30] to equilibrate and establish an optimal complex. Regarding the position of the substituent, the 6-substituted benzofurans (13) and the 4-substituted phenyl derivatives (19) formed more stable complexes than the 5-substituted analogues (14) (Fig. S1).

Studying the binding profile through the simulation time (Fig. S2) and the ligand interactions of the final frame of the MD simulation

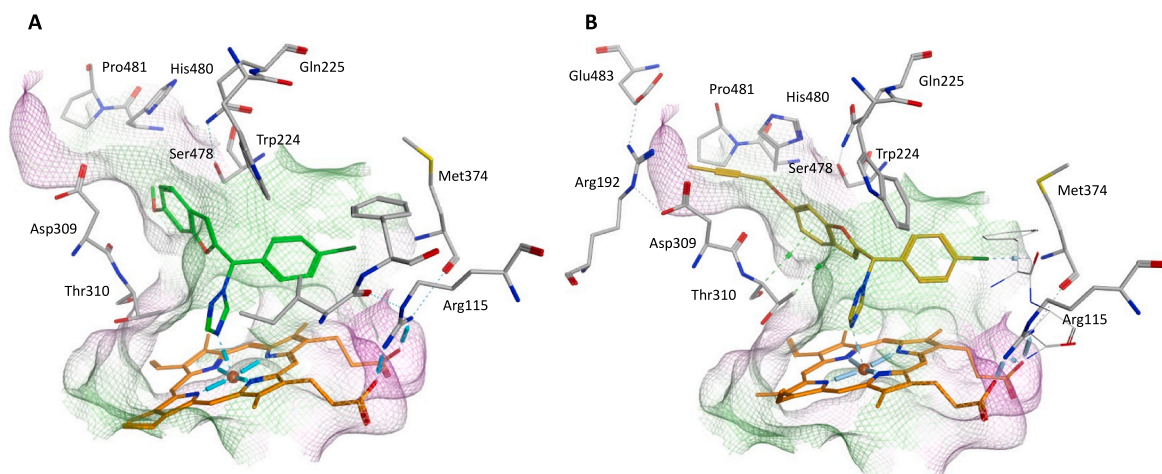


Fig. 5. 3D fitting of the final frame after 150 ns MD simulation in the active site of the aromatase enzyme for (A) the 6-methoxy derivative S-5a (B) the 6-but-2-ynyloxy derivative S-13b.

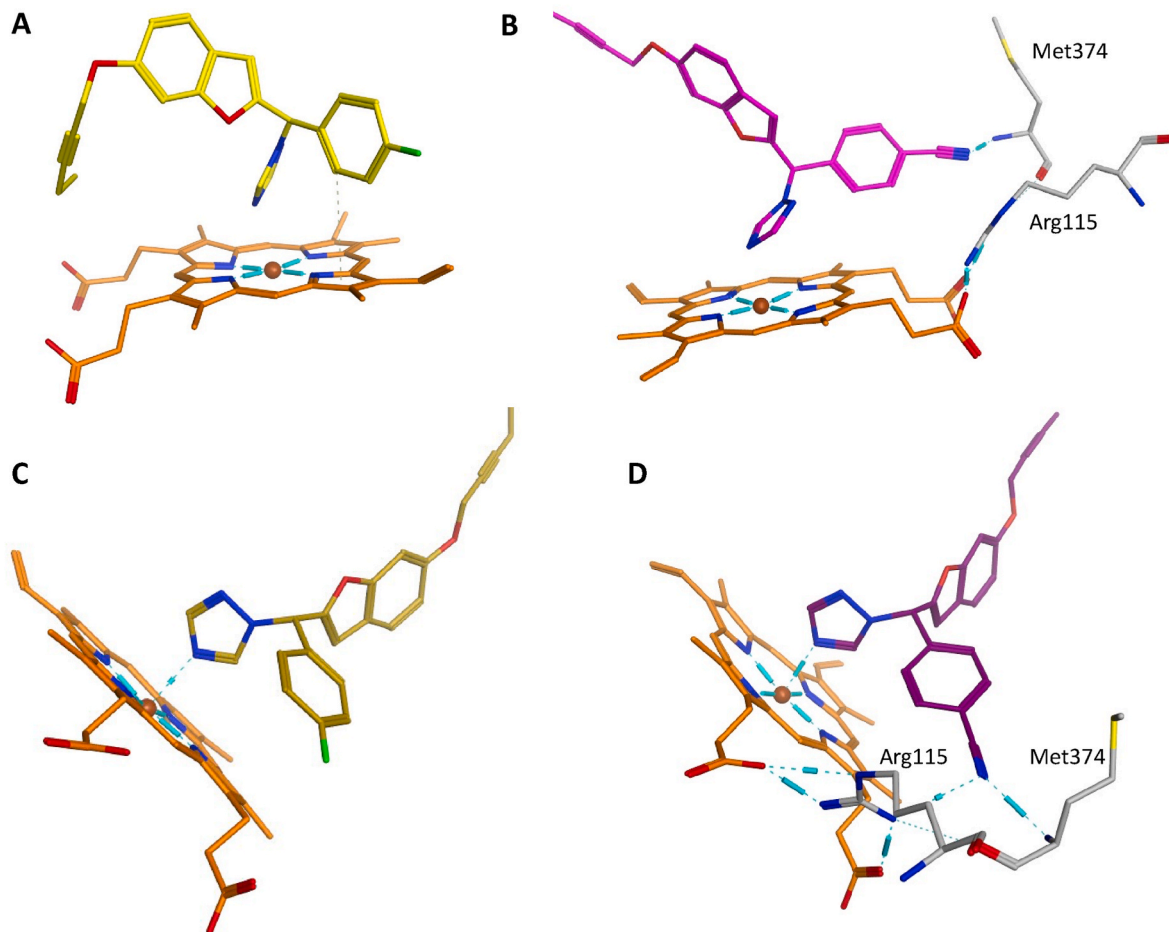


Fig. 6. Positioning of ligands with respect to the haem of the final frame of (A) R-13e (B) S-13e (C) R-13h (D) S-13h after 400 ns MD simulations.

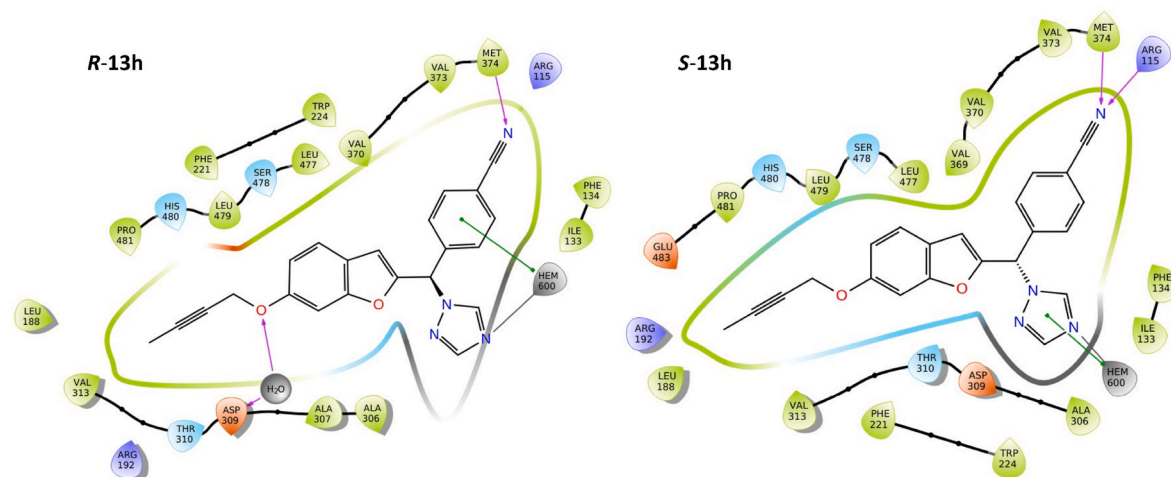


Fig. 7. Protein-ligand interactions of *R*- and *S*-13h within the haem and access channel binding sites of CYP19A1.

(Fig. S3) indicated that both enantiomers of the simpler methoxy derivative (**5a**) can comfortably fit in the haem binding pocket. Introduction of the extended pentynyloxy group restricted fit within the enzyme with the 6-pentynyloxy **S**-13a more optimally positioned for the access channel compared with **R**-13a, although both bind with the haem through the N4 of triazole. For the 5-pentynyloxy benzofurans (e.g. **14**) the *S*-enantiomer also showed a more favourable binding profile, while the *R*-enantiomer of **14** binds to the haem through the N2 of triazole. In contrast, the *R*-enantiomers of the phenyl substituted derivatives (e.g. **19**) bound with the haem through the N4 of the triazole ring, while the *S*-enantiomers bound with the haem through the N2 of the triazole ring. For optimal haem binding the azole should be perpendicular ($\sim 90^\circ$) to the plane of the haem group, which is normally achieved through binding with the N4 of the triazole, however binding via the N2 of the triazole does not allow a perpendicular interaction, which would result in a less favourable conformation for binding.

Varying the length of the alkyl chain substituent at the 6-position of the benzofuran group did not show a significant difference in the stability of the complex and all compounds showed good 3D fitting, with the methoxy derivatives fitting in the haem active site pocket e.g. **5a** (Fig. 5A), and the longer chain substituted derivatives fitting both the haem active site and the access channel gated by Arg192, Asp309, His480 and Glu483 e.g. **13b** (Fig. 5B) with the chloro substituent forming a binding interaction with the key amino acid Met374.

The *S*-enantiomer of the lead compounds, 6-pent-2-ynyloxy 4' fluoro-substituted (**13e**) and 6-but-2-ynyloxy 4' nitrile-substituted derivative (**13h**) were optimally positioned within the haem and access channel binding sites and formed a direct N4-triazole haem binding interaction with a distance of 2.37 and 2.38 Å respectively (Fig. 6C and D). The pent-2-ynyloxy chain of *R*-13e was not optimally positioned in the access channel and, although the triazole N4 was close to the haem iron (2.43 Å) a direct bond was not observed (Fig. 6A). For both enantiomers of **13h** the nitrile group formed binding interactions with Met374 and directly or indirectly with Arg115 (Fig. 6B and D) and the but-2-ynyloxy chain was optimally positioned within the access channel.

3. Conclusion

The 6-*O*-alkyl/alkyne benzofurans (**5**, **13**) were optimal with respect to aromatase inhibitory activity compared with the 5-*O*-alkyl/alkyne benzofurans (**6**, **14**) and 4'-*O*-alkyl/alkyne phenyl derivatives (**7**, **19**) (Table 1) and the 6-*O*-alkyl/alkyne benzofurans equilibrated with more stable aromatase-ligand complexes over the MD simulations (Fig. S1). Further investigation of the 6-*O*-alkyl/alkyne benzofuran derivatives with either Cl, F or CN substitutions in the 4'-position of the phenyl ring

determined that the 6-*O*-but-2-yne chain was optimal for aromatase inhibitory activity of the chloro (**13b**) and nitrile (**13h**) substituted phenyl rings (IC_{50} 0.53 and 0.09 nM respectively), while the 6-*O*-pent-2-yne chain was optimal for aromatase inhibitory activity of the F (**13e**) substituted phenyl ring (IC_{50} 0.51 nM) (Table 3). Computational studies indicated that the alkyne chain was positioned in the front door access channel gated by Arg192, Asp309, His480 and Glu483 with additional stabilizing hydrophobic interactions. Binding interaction with Met374 was also noted for the chloro (**13b**) and nitrile (**13h**) derivatives (Fig. 6 and S3).

From computational studies it is proposed that the improved aromatase inhibitory activity of the nitrile derivative (**13h**) may be owing to the ability of both *R*- and *S*-enantiomers to fit optimally within both binding pockets and interact with the haem through the N4 of the triazole ring with anchoring of the ligands through a H-bonding interaction between CN and Met374/Arg115 (Fig. 7), and future experimental studies will involve experimental studies to validate the computational findings. The excellent toxicity and selectivity profile of these compounds also supports the basis and rationale for continuing research, subject to funding, for these 4th generation nonsteroidal aromatase inhibitors.

4. Experimental section

4.1. Materials and instrumentation for the chemical synthesis

All commercially available starting materials and solvents were of general purpose or analytical grade and used without further purification. Melting points were determined using a Gallenkamp melting point apparatus and are uncorrected. ^1H and ^{13}C NMR spectra were recorded on a Bruker Advance DP500 spectrometer operating at 500 MHz and 125 MHz, respectively. Chemical shifts are given in parts per million (ppm) relative to the internal standard tetramethylsilane (Me_4Si). Analytical thin layer chromatography (TLC) was carried out on pre-coated silica plates (ALUGRAM® SIL G/UV254) with visualisation via UV light (254 nm). HPLC were either performed by the Department of Pharmacy & Pharmacology, University of Bath, Bath, UK on a Zorbax Eclipse plus C18 Rapid resolution 2.1×50 mm, $1.8 \mu\text{m}$ particle size using gradient (methanol: H_2O) with 0.1% formic acid (method A) or in house on a Shimadzu LC-2030C Plus C18 Rapid resolution 250×4.6 mm, $5 \mu\text{m}$ particle size using isocratic 80:20 (methanol: H_2O) (method B). All biologically evaluated compounds are $\geq 95\%$ pure by HPLC analysis.

Methods for the preparation of the ketones (**3**, **9**), alcohols (**4**, **10**, **17**) and compounds **15** and **16** are described in the Supporting

information. Triazoles **5a-c**, **11a** and **11c** were previously reported by us [23].

4.2. General method for the preparation of the 1-(substituted benzofuran-2-yl)(4-substituted phenyl)methyl-1H-1,2,4-triazole (**5**, **6**, **7**, **11**, **12** and **18**)

To a cooled suspension of triazole (4 m.eq.) in dry CH₃CN (3 mL/mmol of the carbinol (**4**, **10** or **17**)) was added a solution of thionyl chloride (1.6 m.eq.) in dry CH₃CN (2 mL/mmol of carbinol). The mixture was stirred at 0 °C for 1 h then K₂CO₃ (1 m.eq.) was added followed by a solution of the carbinol (**4**, **10** or **17**) (1 m.eq.) in dry CH₃CN (3 mL/mmol of carbinol) and the reaction stirred at room temperature for 16 h. The reaction mixture was then filtered to remove any insoluble substances. The filtrate was diluted with EtOAc (100 mL) and washed with H₂O (3 × 50 mL). The organic layer was dried (MgSO₄) and concentrated under reduced pressure.

1-((4-Chlorophenyl)(5-methoxybenzofuran-2-yl)methyl)-1H-1,2,4-triazole (6**)**. Prepared from (4-chlorophenyl)(5-methoxybenzofuran-2-yl)methanol (**4b**) (0.3 g, 1.04 mmol). Purification by gradient column chromatography afforded the product (**6**) at 60% EtOAc in petroleum ether (v/v) as a yellow oil. Yield: 0.26 g (63%); *R*_f = 0.1 (petroleum ether - EtOAc 3:1 v/v). ¹H NMR (CDCl₃): δ 8.16 (s, 1H, CH-triazole), 8.05 (s, 1H, CH-triazole), 7.41 (d, *J* = 8.6 Hz, 2H, Ar), 7.37 (d, *J* = 8.9 Hz, 1H, Ar), 7.25 (d, *J* = 8.4 Hz, 2H, Ar), 7.01 (d, *J* = 2.6 Hz, 1H, Ar), 6.96 (dd, *J* = 2.6, 8.9 Hz, 1H, Ar), 6.81 (s, 1H, Ar), 6.55 (s, 1H, CH), 3.84 (s, 3H, OCH₃). ¹³C NMR (CDCl₃): δ 156.38 (C), 152.66 (C), 152.36 (CH), 150.35 (C), 143.26 (CH), 135.25 (C), 134.22 (C), 129.33 (2 x CH), 129.02 (2 x CH), 127.92 (C), 114.33 (CH), 112.08 (CH), 108.14 (CH), 103.82 (CH), 61.57 (CH), 55.93 (CH₃). HPLC (A): 99.9% at R.T. = 8.9 min.

1-((5-Chlorobenzofuran-2-yl)(4-methoxyphenyl)methyl)-1H-1,2,4-triazole (7**)**. Prepared from (5-chlorobenzofuran-2-yl)(4-methoxyphenyl)methanol (**4c**) [23] (0.5 g, 1.74 mmol). Purification by gradient column chromatography afforded the product (**7**) at 60% EtOAc in petroleum ether (v/v) as a yellow oil. Yield: 0.18 g (31%); *R*_f = 0.25 (petroleum ether - EtOAc 3:1 v/v). ¹H NMR (CDCl₃): δ 8.30 (s, 1H, CH-triazole), 8.01 (s, 1H, CH-triazole), 7.43 (d, *J* = 1.7 Hz, 1H, Ar), 7.30 (d, *J* = 8.6 Hz, 1H, Ar), 7.23 (d, *J* = 8.7 Hz, 2H, Ar), 7.20 (dd, obscured by CDCl₃, 1H, Ar), 6.88 (d, *J* = 8.7 Hz, 2H, Ar), 6.75 (s, 1H, Ar), 6.45 (s, 1H, CH), 3.75 (s, 3H, OCH₃). ¹³C NMR (CDCl₃): δ 160.47 (C), 154.29 (C), 153.66 (C), 151.06 (CH), 129.35 (2 x CH), 128.99 (C), 128.84 (C), 126.64 (C), 125.51 (CH), 121.08 (CH), 114.66 (2 x CH), 112.56 (CH), 107.08 (CH), 62.02 (CH), 56.35 (CH₃). HPLC (B): 97.8% at R.T. = 6.33 min.

2-((4-Fluorophenyl)(1H-1,2,4-triazol-1-yl)methyl)benzofuran-6-ol (11b**, R³ = F)**. Prepared from (4-fluorophenyl)(6-((tetrahydro-2H-pyran-2-yl)oxy)benzofuran-2-yl)methanol (**10c**) [23] (0.71 g, 1.97 mmol). Purification by gradient column chromatography afforded the product (**11b**) at 70% EtOAc in petroleum ether (v/v) as a yellow wax. Yield: 0.46 g (86%); *R*_f = 0.22 (petroleum ether - EtOAc 1:1 v/v). ¹H NMR (DMSO-*d*₆): δ 9.61 (bs, 1H, OH), 8.70 (s, 1H, CH-triazole), 8.08 (s, 1H, CH-triazole), 7.52 (m, 2H, Ar), 7.38 (d, *J* = 8.5 Hz, 1H, Ar), 7.29 (t, *J* = 8.9 Hz, 3H, Ar), 6.75 (d, *J* = 1.9 Hz, 1H, Ar), 6.75 (dd, *J* = 2.1, 8.4 Hz, 1H, Ar), 6.49 (t, *J* = 1.0 Hz, 1H, CH). ¹³C NMR (DMSO-*d*₆): δ 161.42 (C), 159.47 (C), 154.34 (C), 154.18 (C), 150.32 (CH), 150.08 (C), 142.53 (CH), 131.14 (C), 128.49 (CH), 128.42 (CH), 120.01 (CH), 117.60 (C), 114.10 (CH), 113.93 (CH), 110.90 (CH), 105.35 (CH), 95.91 (CH), 57.77 (CH). HPLC (B): 98.3% at R.T. = 4.04 min.

2-((4-Chlorophenyl)(1H-1,2,4-triazol-1-yl)methyl)benzofuran-5-ol (12**)**. Prepared from (4-chlorophenyl)(5-((tetrahydro-2H-pyran-2-yl)oxy)benzofuran-2-yl)methanol (**10b**) [23] (0.71 g, 1.97 mmol). Purification by gradient column chromatography afforded the product (**12**) at 70% EtOAc in petroleum ether (v/v) as a thick yellow oil. Yield: 0.5 g (78%); *R*_f = 0.2 (petroleum ether - EtOAc 1:1 v/v). ¹H NMR (DMSO-*d*₆): δ 9.22 (bs, 1H, OH), 8.72 (s, 1H, CH-triazole), 8.09 (s, 1H,

CH-triazole), 7.52 (d, *J* = 8.6 Hz, 2H, Ar), 7.47 (d, *J* = 8.5 Hz, 2H, Ar), 7.33 (m, 2H, Ar), 6.92 (d, *J* = 2.46 Hz, 1H, Ar), 6.75 (dd, *J* = 2.5, 8.7 Hz, 1H, Ar), 6.51 (t, *J* = 0.95 Hz, 1H, CH). ¹³C NMR (DMSO-*d*₆): δ 154.20 (C), 153.97 (C), 152.53 (CH), 149.23 (C), 144.82 (CH), 135.83 (C), 133.94 (C), 130.30 (2 x CH), 129.32 (2 x CH), 128.62 (C), 114.19 (CH), 111.94 (CH), 107.47 (CH), 106.32 (CH), 59.86 (CH). HPLC (B): 95.6% at R.T. = 4.36 min.

4-((5-Chlorobenzofuran-2-yl)(1H-1,2,4-triazol-1-yl)methyl)phenol (18**)**. Prepared from (5-chlorobenzofuran-2-yl)(4-((tetrahydro-2H-pyran-2-yl)oxy)phenyl)methanol (**17**) (0.47 g, 1.31 mmol). Purification by gradient column chromatography afforded the product (**18**) at 70% EtOAc in petroleum ether (v/v) as a white solid. Yield: 0.19 g (45%); m.p. 240–242 °C; *R*_f = 0.17 (petroleum ether - EtOAc 1:1 v/v). ¹H NMR (DMSO-*d*₆): δ 9.69 (bs, 1H, OH), 8.68 (s, 1H, CH-triazole), 8.06 (s, 1H, CH-triazole), 7.71 (d, *J* = 2.1 Hz, 1H, Ar), 7.59 (d, *J* = 8.7 Hz, 1H, Ar), 7.34 (dd, *J* = 2.2, 8.7 Hz, 1H, Ar), 7.31 (d, *J* = 8.6 Hz, 2H, Ar), 7.20 (s, 1H, Ar), 6.81 (d, *J* = 8.6 Hz, 1H, Ar), 6.61 (t, *J* = 1.0 Hz, 1H, CH). ¹³C NMR (DMSO-*d*₆): δ 158.36 (C), 156.80 (C), 153.49 (C), 152.37 (CH), 144.55 (CH), 129.91 (2 x CH), 129.67 (C), 127.96 (C), 126.68 (C), 125.21 (CH), 121.46 (CH), 115.97 (2 x CH), 113.31 (CH), 106.75 (CH), 60.15 (CH). HPLC (B): 100% at R.T. = 4.69 min.

4.3. General method for the preparation of the longer chain 1-(substituted benzofuran-2-yl)(4-substituted phenyl)methyl-1H-1,2,4-triazole (**13**, **14** and **19**)

To a solution of the phenolic compound (**11**, **12** or **18**) (1 m.eq.) in dry CH₃CN (13 mL/mmol of phenolic compound), K₂CO₃ (1.2 m.eq.) was added and the mixture stirred for 1 h at 40 °C then the alkyl/alkyne bromide (1.2–6 m.eq.) was added and the reaction mixture stirred at room temperature for 16 h. The reaction mixture was concentrated under reduced pressure and the residue dissolved in EtOAc (100 mL), washed with H₂O (3 × 50 mL), dried (MgSO₄) and concentrated under reduced pressure.

1-((4-Chlorophenyl)(6-(pent-2-yn-1-yloxy)benzofuran-2-yl)methyl)-1H-1,2,4-triazole (13a**, R = pent-2-yne, R³ = Cl)**. Prepared from 2-((4-chlorophenyl)(1H-1,2,4-triazol-1-yl)methyl)benzofuran-6-ol (**11a**) [23] (0.2 g, 0.61 mmol) and 1-bromopent-2-yne (0.07 mL, 0.67 mmol). Purification by gradient column chromatography afforded the product (**13a**) at 60% EtOAc in petroleum ether (v/v) as a yellow oil. Yield: 0.18 g (75%); *R*_f = 0.55 (petroleum ether - EtOAc 1:1 v/v). ¹H NMR (CDCl₃): δ 8.24 (s, 1H, CH-triazole), 7.98 (s, 1H, CH-triazole), 7.34 (m, 3H, Ar), 7.17 (d, *J* = 8.4 Hz, 2H, Ar), 7.00 (d, *J* = 2.0 Hz, 1H, Ar), 6.87 (dd, *J* = 2.1, 8.5 Hz, 1H, Ar), 6.75 (s, 1H, Ar), 6.45 (s, 1H, CH), 4.62 (t, *J* = 2.1 Hz, 2H, CH₂), 2.16 (qt, *J* = 2.1, 7.5 Hz, 2H, CH₂), 1.07 (t, *J* = 7.5 Hz, 3H, CH₃). ¹³C NMR (CDCl₃): δ 156.98 (C), 156.26 (C), 151.81 (CH), 150.87 (C), 143.19 (CH), 135.27 (C), 134.17 (C), 129.33 (2 x CH), 128.08 (2 x CH), 121.50 (CH), 120.98 (C), 113.44 (CH), 108.20 (CH), 97.37 (CH), 89.98 (C), 73.87 (C), 61.70 (CH), 57.11 (CH₂), 13.59 (CH₃), 12.51 (CH₂). HPLC (A): 99% at R.T. = 4.89 min.

1-((6-(But-2-yn-1-yloxy)benzofuran-2-yl)(4-chlorophenyl)methyl)-1H-1,2,4-triazole (13b**, R = but-2-yne, R³ = Cl)**. Prepared from 2-((4-chlorophenyl)(1H-1,2,4-triazol-1-yl)methyl)benzofuran-6-ol (**11a**) [23] (0.22 g, 0.67 mmol) and 1-bromobut-2-yne (0.12 mL, 1.35 mmol). Purification by gradient column chromatography afforded the product (**13b**) at 60% EtOAc in petroleum ether (v/v) as a yellow oil. Yield: 0.19 g (76%); *R*_f = 0.3 (petroleum ether - EtOAc 1:1 v/v). ¹H NMR (CDCl₃): δ 8.15 (s, 1H, CH-triazole), 8.05 (s, 1H, CH-triazole), 7.44 (d, *J* = 8.6 Hz, 1H, Ar), 7.41 (d, *J* = 8.5 Hz, 2H, Ar), 7.25 (d, *J* = 8.2 Hz, 2H, Ar), 7.10 (d, *J* = 2.1 Hz, 1H, Ar), 6.96 (dd, *J* = 2.2, 8.6 Hz, 1H, Ar), 6.81 (s, 1H, Ar), 6.54 (t, *J* = 0.8 Hz, 1H, CH), 4.70 (q, *J* = 2.2 Hz, 2H, CH₂), 1.89 (t, *J* = 2.3 Hz, 3H, CH₃). ¹³C NMR (CDCl₃): δ 156.91 (C), 156.25 (C), 152.38 (CH), 151.05 (C), 143.26 (CH), 135.20 (C), 134.33 (C), 129.31 (2 x CH), 128.94 (2 x CH), 121.72 (CH), 121.01 (C), 113.39 (CH), 108.08 (CH), 97.29 (CH), 84.17 (C), 73.71 (C), 61.56 (CH), 57.01 (CH₂), 3.74 (CH₃). HPLC (B): 100% at R.T. = 7.35 min.

1-((4-Chlorophenyl)(6-ethoxybenzofuran-2-yl)methyl)-1H-1,2,4-triazole (13c, R = ethyl R³ = Cl). Prepared from 2-((4-chlorophenyl)(1H-1,2,4-triazol-1-yl)methyl)benzofuran-6-ol (**11a**) [23] (0.2 g, 0.61 mmol) and ethylbromide (0.25 mL, 3.4 mmol). Purification by gradient column chromatography afforded the product (**13c**) at 60% EtOAc in petroleum ether (v/v) as a yellow oil. Yield: 0.147 g (67%); *R_f* = 0.4 (petroleum ether - EtOAc 1:1 v/v). ¹H NMR (CDCl₃): δ 8.05 (s, 1H, CH-triazole), 7.94 (s, 1H, CH-triazole), 7.32 (m, 3H, Ar), 7.14 (d, *J* = 8.2 Hz, 2H, Ar), 6.89 (d, *J* = 2.1 Hz, 1H, Ar), 6.81 (dd, *J* = 2.2, 8.6 Hz, 1H, Ar), 6.70 (s, 1H, Ar), 6.42 (t, *J* = 0.9 Hz, 1H, CH), 3.99 (q, *J* = 6.9 Hz, 2H, CH₂), 1.37 (t, *J* = 6.9 Hz, 3H, CH₃). ¹³C NMR (CDCl₃): δ 158.10 (C), 156.50 (C), 152.35 (CH), 150.68 (C), 143.22 (CH), 135.15 (C), 134.41 (C), 129.28 (2 x CH), 128.92 (2 x CH), 121.67 (CH), 120.36 (C), 113.24 (CH), 108.12 (CH), 96.56 (CH), 64.02 (CH₂), 61.57 (CH), 14.77 (CH₃). HPLC (B): 100% at R.T. = 7.56 min.

1-((4-Chlorophenyl)(6-(prop-2-yn-1-yloxy)benzofuran-2-yl)methyl)-1H-1,2,4-triazole (13d, R = prop-2-yn R³ = Cl). Prepared from 2-((4-chlorophenyl)(1H-1,2,4-triazol-1-yl)methyl)benzofuran-6-ol (**11a**) [23] (0.2 g, 0.61 mmol) and propargylbromide (80% wt in toluene) (0.2 mL, 1.84 mmol). Purification by gradient column chromatography afforded the product (**13d**) at 60% EtOAc in petroleum ether (v/v) as a yellow oil. Yield: 0.2 g (90%); *R_f* = 0.37 (petroleum ether - EtOAc 1:1 v/v). ¹H NMR (CDCl₃): δ 8.06 (s, 1H, CH-triazole), 7.95 (s, 1H, CH-triazole), 7.36 (d, *J* = 8.6 Hz, 1H, Ar), 7.32 (d, *J* = 8.5 Hz, 2H, Ar), 7.15 (d, *J* = 8.4 Hz, 2H, Ar), 7.02 (d, *J* = 2.1 Hz, 1H, Ar), 6.88 (dd, *J* = 2.3, 8.5 Hz, 1H, Ar), 6.71 (s, 1H, Ar), 6.45 (t, *J* = 0.9 Hz, 1H, CH), 4.65 (d, *J* = 2.4 Hz, 2H, CH₂), 2.47 (t, *J* = 2.4 Hz, 1H, CH). ¹³C NMR (CDCl₃): δ 156.55 (C), 156.15 (C), 152.39 (CH), 151.29 (C), 143.23 (CH), 135.23 (C), 134.27 (C), 129.32 (2 x CH), 128.95 (2 x CH), 121.83 (CH), 121.36 (C), 113.35 (CH), 108.02 (CH), 97.52 (CH), 78.24 (C), 75.93 (CH), 61.53 (CH), 56.41 (CH₂). HPLC (B): 100% at R.T. = 5.78 min.

1-((4-Fluorophenyl)(6-(pent-2-yn-1-yloxy)benzofuran-2-yl)methyl)-1H-1,2,4-triazole (13e, R = pent-2-yn R³ = F). Prepared from 2-((4-fluorophenyl)(1H-1,2,4-triazol-1-yl)methyl)benzofuran-6-ol (**11b**) (0.2 g, 0.64 mmol) and 1-bromopent-2-yne (0.13 mL, 1.29 mmol). Purification by gradient column chromatography afforded the product (**13e**) at 60% EtOAc in petroleum ether (v/v) as a yellow oil. Yield: 0.12 g (50%); *R_f* = 0.43 (petroleum ether - EtOAc 1:1 v/v). ¹H NMR (DMSO-*d*₆): δ 8.72 (s, 1H, CH-triazole), 8.08 (s, 1H, CH-triazole), 7.54 (m, 3H, Ar), 7.32 (s, 1H, Ar), 7.30 (t, *J* = 8.9 Hz, 2H, Ar), 7.21 (d, *J* = 1.9 Hz, 1H, Ar), 6.91 (dd, *J* = 2.2, 8.5 Hz, 1H, Ar), 6.56 (t, *J* = 0.9 Hz, 1H, CH), 4.77 (t, *J* = 2.1 Hz, 2H, CH₂), 2.24 (qt, *J* = 2.2, 7.5 Hz, 2H, CH₂), 1.06 (t, *J* = 7.5 Hz, 3H, CH₃). ¹³C NMR (DMSO-*d*₆): δ 163.57 (C), 161.62 (C), 156.52 (C), 155.89 (C), 153.26 (C), 152.49 (CH), 144.71 (CH), 133.15 (C), 130.67 (CH), 130.60 (CH), 122.20 (CH), 121.40 (C), 116.26 (CH), 116.08 (CH), 113.22 (CH), 107.33 (CH), 97.65 (CH), 89.58 (C), 75.27 (C), 59.79 (CH), 56.93 (CH₂), 13.98 (CH₃), 12.14 (CH₂). HPLC (B): 100% at R.T. = 6.70 min.

1-((4-Fluorophenyl)(6-(but-2-yn-1-yloxy)benzofuran-2-yl)methyl)-1H-1,2,4-triazole (13f, R = but-2-yn R³ = F). Prepared from 2-((4-fluorophenyl)(1H-1,2,4-triazol-1-yl)methyl)benzofuran-6-ol (**11b**) (0.17 g, 0.57 mmol) and 1-bromobut-2-yne (0.1 mL, 1.12 mmol). Purification by gradient column chromatography the product (**13f**) at 60% EtOAc in petroleum ether (v/v), which was further purified by preparative TLC to afford the product as a yellow oil. Yield: 0.07 g (36%); *R_f* = 0.50 (petroleum ether - EtOAc 1:1 v/v). ¹H NMR (CDCl₃): δ 8.16 (s, 1H, CH-triazole), 8.05 (s, 1H, CH-triazole), 7.44 (d, *J* = 8.6 Hz, 1H, Ar), 7.32 (m, 2H, Ar), 7.15 (m, 3H, Ar), 6.96 (dd, *J* = 2.2, 8.5 Hz, 1H, Ar), 6.81 (s, 1H, CH), 6.52 (t, *J* = 0.9 Hz, 1H, Ar), 4.70 (q, *J* = 2.3 Hz, 2H, CH₂), 1.89 (t, *J* = 2.3 Hz, 3H, CH₃). ¹³C NMR (CDCl₃): δ 163.99 (d, ¹*J*_{C,F} = 247.51 Hz, C), 156.87 (C), 156.23 (C), 152.29 (CH), 151.36 (C), 143.03 (CH), 131.64 (d, ⁴*J*_{C,F} = 3.36 Hz, C), 129.53 (d, ³*J*_{C,F} = 8.40 Hz, 2 x CH), 121.69 (CH), 121.05 (C), 116.22 (d, ²*J*_{C,F} = 21.75 Hz, 2 x CH), 113.34 (CH), 107.92 (CH), 97.30 (CH), 84.15 (C), 73.72 (C), 61.56 (CH), 57.01 (CH₂), 3.74 (CH₃). HPLC (A): 99.0% at R.T. = 4.73 min.

4-((6-(Pent-2-yn-1-yloxy)benzofuran-2-yl)(1H-1,2,4-triazol-1-

yl)methyl)benzonitrile (13g, R = pent-2-yn R³ = CN). Prepared from 4-((6-hydroxybenzofuran-2-yl)(1H-1,2,4-triazol-1-yl)methyl)benzonitrile (**11c**) [23] (0.1 g, 0.31 mmol) and 1-bromopent-2-yne (0.07 mL, 0.68 mmol). Purification by gradient column chromatography afforded the product (**13g**) at 70% EtOAc in petroleum ether (v/v) as a yellow oil. Yield: 0.02 g (17%); *R_f* = 0.27 (petroleum ether - EtOAc 1:1 v/v). ¹H NMR (CDCl₃): δ 8.11 (s, 1H, CH-triazole), 7.98 (s, 1H, CH-triazole), 7.64 (d, *J* = 8.5 Hz, 2H, Ar), 7.36 (d, *J* = 8.6 Hz, 1H, Ar), 7.30 (d, *J* = 8.2 Hz, 2H, Ar), 7.02 (d, *J* = 1.99 Hz, 1H, Ar), 6.89 (dd, *J* = 2.1, 8.5 Hz, 1H, Ar), 6.78 (s, 1H, Ar), 6.49 (app. s, 1H, CH), 4.63 (t, *J* = 2.1 Hz, 2H, CH₂), 2.19 (qt, *J* = 2.1, 7.5 Hz, 2H, CH₂), 1.08 (t, *J* = 7.5 Hz, 3H, CH₃). ¹³C NMR (CDCl₃): δ 157.18 (C), 156.34 (C), 152.63 (CH), 149.86 (C), 140.95 (C), 132.82 (2 x CH), 128.23 (2 x CH), 121.83 (CH), 120.78 (C), 118.06 (C), 113.65 (CH), 113.16 (C), 108.63 (CH), 97.35 (CH), 90.04 (C), 73.79 (C), 61.60 (CH), 57.11 (CH₂), 13.58 (CH₃), 12.51 (CH₂). HPLC (B): 97.4% at R.T. = 5.45 min.

4-((6-(But-2-yn-1-yloxy)benzofuran-2-yl)(1H-1,2,4-triazol-1-yl)methyl)benzonitrile (13h, R = but-2-yn R³ = CN). Prepared from 4-((6-hydroxybenzofuran-2-yl)(1H-1,2,4-triazol-1-yl)methyl)benzonitrile (**11c**) [23] (0.2 g, 0.63 mmol) and 1-bromobut-2-yne (0.11 mL, 1.26 mmol). Purification by gradient column chromatography at 70% EtOAc in petroleum ether (v/v), followed by preparative TLC afforded the product (**13h**) as a yellow oil. Yield: 0.017 g (7%); *R_f* = 0.27 (Petroleum ether/ethyl acetate 1:1). ¹H NMR (CDCl₃): δ 8.11 (s, 1H, CH-triazole), 7.98 (s, 1H, CH-triazole), 7.64 (d, *J* = 8.5 Hz, 2H, Ar), 7.36 (d, *J* = 8.6 Hz, 1H, Ar), 7.30 (d, *J* = 8.2 Hz, 2H, Ar), 7.02 (d, *J* = 2.2 Hz, 1H, Ar), 6.89 (dd, *J* = 2.3, 8.6 Hz, 1H, Ar), 6.78 (s, 1H, Ar), 6.49 (s, 1H, CH), 4.62 (q, *J* = 2.3 Hz, 2H, CH₂), 1.80 (t, *J* = 2.3 Hz, 3H, CH₃). ¹³C NMR (CDCl₃): δ 176.61 (C), 157.13 (C), 156.33 (C), 149.85 (C), 140.94 (C), 132.82 (2 x CH), 128.23 (2 x CH), 121.86 (CH), 120.66 (C), 118.06 (C), 113.62 (CH), 113.15 (C), 108.62 (CH), 97.28 (CH), 84.27 (C), 73.57 (C), 61.60 (CH), 57.01 (CH₂), 3.74 (CH₃). HPLC (A): 98.6% at R.T. = 4.60 min.

1-((4-Chlorophenyl)(5-(pent-2-yn-1-yloxy)benzofuran-2-yl)methyl)-1H-1,2,4-triazole (14). Prepared from 2-((4-chlorophenyl)(1H-1,2,4-triazol-1-yl)methyl)benzofuran-5-ol (**12**) (0.2 g, 0.61 mmol) and 1-bromopent-2-yne (0.07 mL, 0.67 mmol). Purification by gradient column chromatography afforded the product (**14**) at 60% EtOAc in petroleum ether (v/v) as a yellow oil. Yield: 0.12 g (50%); *R_f* = 0.42 (petroleum ether - EtOAc 1:1 v/v). ¹H NMR (CDCl₃): δ 8.70 (s, 1H, CH-triazole), 8.08 (s, 1H, CH-triazole), 7.34 (d, *J* = 8.3 Hz, 2H, Ar), 7.28 (d, *J* = 9.1 Hz, 1H, Ar), 7.25 (d, *J* = 8.3 Hz, 2H, Ar), 7.02 (d, *J* = 2.6 Hz, 1H, Ar), 6.94 (dd, *J* = 2.6, 9.0 Hz, 1H, Ar), 6.86 (s, 1H, Ar), 6.51 (s, 1H, CH), 4.60 (t, *J* = 2.2 Hz, 2H, CH₂), 2.18 (qt, *J* = 2.1, 7.5 Hz, 2H, CH₂), 1.07 (t, *J* = 7.5 Hz, 3H, CH₃). ¹³C NMR (CDCl₃): δ 156.62 (C), 151.90 (C), 150.72 (C), 135.66 (C), 133.38 (C), 129.46 (2 x CH), 129.28 (2 x CH), 127.74 (C), 115.37 (CH), 112.11 (CH), 108.66 (CH), 105.64 (CH), 89.69 (C), 74.16 (C), 62.16 (CH), 57.38 (CH₂), 13.62 (CH₃), 12.50 (CH₂). HPLC (A): 97.7% at R.T. = 4.89 min.

1-((5-Chlorobenzofuran-2-yl)(4-(pent-2-yn-1-yloxy)phenyl)methyl)-1H-1,2,4-triazole (19). Prepared from 2 4-((5-chlorobenzofuran-2-yl)(1H-1,2,4-triazol-1-yl)methyl)phenol (**18**) (0.15 g, 0.69 mmol) and 1-bromopent-2-yne (0.07 mL, 0.67 mmol). Purification by gradient column chromatography afforded the product (**19**) at 60% EtOAc in petroleum ether (v/v) as a yellow oil. Yield: 0.08 g (44%); *R_f* = 0.42 (petroleum ether - EtOAc 1:1 v/v). ¹H NMR (CDCl₃): δ 8.21 (s, 1H, CH-triazole), 7.99 (s, 1H, CH-triazole), 7.43 (d, *J* = 1.9 Hz, 1H, Ar), 7.30 (d, *J* = 8.7 Hz, 1H, Ar), 7.22 (m, 3H, Ar), 6.95 (d, *J* = 8.8 Hz, 2H, Ar), 6.73 (s, 1H, Ar), 6.45 (s, 1H, CH), 4.61 (t, *J* = 2.1 Hz, 2H, CH₂), 2.18 (qt, *J* = 2.1, 7.5 Hz, 2H, CH₂), 1.07 (t, *J* = 7.5 Hz, 3H, CH₃). ¹³C NMR (CDCl₃): δ 158.71 (C), 154.33 (C), 153.66 (C), 151.39 (CH), 142.96 (CH), 129.24 (2 x CH), 128.99 (C), 128.84 (C), 127.26 (C), 125.50 (CH), 121.08 (CH), 115.57 (2 x CH), 112.56 (CH), 107.07 (CH), 90.06 (C), 73.71 (C), 61.91 (CH), 56.63 (CH₂), 13.57 (CH₃), 12.49 (CH₂). HPLC: (B) 96.1% at R.T. = 9.17 min.

4.4. Computational studies

4.4.1. Docking

The crystal structure of human placental aromatase (CYP19A1) refined at 2.75 Å (PDB 3S79) [21], was downloaded from the protein data bank (<https://www.rcsb.org>). Missing hydrogens were added, and the charge and geometry of the iron atom were adjusted as previously described [31]. Using the site finder tool in molecular operating environment (MOE) 2015-10 software [28], the active site was chosen to contain the main amino acid residues and the haem molecule. The amino acids constituting the wall of the active site contained Arg115, Ile133, Phe134, Phe221, Trp224, Ile305, Ala306, Asp309, Thr310, Val370, Leu372, Val373, Met374, Leu477, Ser478. The 3D structures of the ligands (R- and S-enantiomers) were generated using MOE builder, energy minimised and saved in a dataset ready for docking studies. The complexes for molecular dynamics (MD) studies were prepared by docking the compounds using MOE.

4.4.2. Molecular dynamics

Molecular dynamics simulations were performed using Schrödinger 2020–1 Desmond programme [29,30] as previously described [32]. Briefly, using the pdb files containing the selected docking poses, the structures were optimised with protein preparation wizard. The volume of space in which the simulation takes place, the global cell, is built up by regular 3D simulation boxes. The orthorhombic water box allowed for a 10 Å buffer region between protein atoms and box sides. Overlapping water molecules were deleted, and the systems were neutralised with Na⁺ ions and salt concentration 0.15 M. Molecular dynamics (150 ns and 400 ns simulations) were performed using OPLS_2005 forcefield at 300 K and constant pressure (1 bar).

4.5. Cell culture

JEG-3 cells were purchased from ATCC and grown in Eagle's Minimal Essential Medium (EMEM) supplemented with 10% fetal calf serum (FCS). MCF-10A cells were a gift from Prof. Christopher McCabe (University of Birmingham) and were grown in Dulbecco's Modified Eagle Medium (DMEM) supplemented with 20 ng/ml epidermal growth factor (EGF), 100 ng/ml cholera toxin, 0.01 mg/ml insulin, 500 ng/ml hydrocortisone, and 5% horse serum (Sigma). MDA-MB-231 cells were purchased from ATCC and grown in Roswell park Memorial Institute medium (RPMI1690) supplemented with 10% FCS. All cells were cultured at 37 °C under 5% CO₂ in a humidified incubator.

4.6. Aromatase activity assay

Aromatase activity was assayed using a modified titrated water assay as previously reported [28]. JEG-3 cells were grown in 1 mL EMEM to approximately 80% confluence in six-well cell culture plates. Androst-4-ene-3,17-dione-[1β-³H] was dissolved in serum-free cell culture medium and added into each well. Aromatase activity was measured in the absence and presence of inhibitor (0.001pM–100pM). After a 1 h incubation at 37 °C followed by a 5-min incubation on ice, 500 µL of culture medium was taken from each well. Medium was vortexed with 2% dextran-treated charcoal (Sigma-Aldrich) in PBS and centrifuged at 4000 rpm. The supernatant containing the product, [³H] H₂O, was quantified by scintillation counting. Cell protein concentrations were determined using Pierce BCA assay kit (Thermo Fisher Scientific). Aromatase activity results were determined as a concentration of product formed per mg of protein per hour (pmol/mg/h). Results were shown as a % change in activity compared to control. Each data point was measured in triplicates and the error in the IC₅₀ calculations represented as 95% confidence interval.

4.7. BrdU-based cell proliferation assay to assess drug toxicity

MCF-10A and MDA-MB-231 cells were plated onto 96-well microtiter tissue culture plates in RPMI1690 medium at a density of 8×10^3 cells/well (for MCF-10A) or 5×10^3 cells/well (for MDA-MB-231). Groups were treated with either DMSO alone (at no greater than 0.01%) as a vehicle control, or at a dose of 1 µM of inhibitor or doxorubicin control, for 48 h. Effects of drug treatment on cell growth were detected using the BrdU cell proliferation assay (Roche) according to the manufacturer's recommendations. The BrdU colorimetric immunoassay is a quantitative cell proliferation assay based on the measurement of BrdU incorporation during DNA synthesis. After treatments 20 µL/well of BrdU were added to each well, followed by an incubation of 2 h at 37 °C. The cells were subsequently fixed, and the DNA denatured. Anti-BrdU-peroxidase immune complexes were detected by substrate reaction and quantified in an ELISA reader at 370 nm.

Notes

The authors declare no competing financial interest.

Declaration of competing interest

The authors declare that they have no known competing financial interests or personal relationships that could have appeared to influence the work reported in this paper.

Acknowledgment

We thank the Egyptian Ministry of Higher Education-Mission Sector and Zagazig University, Egypt for funding this research in Cardiff University through a PhD scholarship to Ahmed Eissa. Molecular dynamics simulations were undertaken using the supercomputing facilities at Cardiff University operated by Advanced Research Computing at Cardiff (ARCCA) on behalf of the Cardiff Supercomputing Facility and the HPC Wales and Supercomputing Wales (SCW) projects. We acknowledge support of the latter, which is part-funded by the European Regional Development Fund (ERDF) via the Welsh Government.

Appendix A. Supplementary data

Supplementary data to this article can be found online at <https://doi.org/10.1016/j.ejmech.2022.114569>.

References

- [1] T. Vargo-Gogola, J.M. Rosen, Modelling breast cancer: one size does not fit all, *Nat. Rev. Cancer* 7 (9) (2007) 659–672, <https://doi.org/10.1038/nrc2193>.
- [2] K. Polyak, Heterogeneity in breast cancer, *J. Clin. Invest.* 121 (10) (2011) 3786–3788, <https://doi.org/10.1172/JCI60534.3786>.
- [3] J. Ferlay, I. Soerjomataram, R. Dikshit, S. Eser, C. Mathers, M. Rebelo, D.M. Parkin, D. Forman, F. Bray, Cancer incidence and mortality worldwide: sources, methods and major patterns in GLOBOCAN 2012, *Int. J. Cancer* 136 (5) (2015) E359–E386, <https://doi.org/10.1002/ijc.29210>.
- [4] Cancer Research UK, Breast cancer statistics. <http://www.wcrf.org/int/cancer-facts-figures/data-specific-cancers/breast-cancer-statistics>. (Accessed 19 December 2021).
- [5] F. Bray, J. Ferlay, I. Soerjomataram, R.L. Siegel, L.A. Torre, A. Jemal, Global cancer statistics 2018: GLOBOCAN estimates of incidence and mortality worldwide for 36 cancers in 185 countries, *CA A Cancer J. Clin.* 68 (6) (2018) 394–424, <https://doi.org/10.3322/caac.21492>.
- [6] J. Ferlay, M. Ervik, F. Lam, M. Colombet, L. Mery, M. Piñeros, A. Znaor, I. Soerjomataram, F. Bray, Global cancer observatory: cancer Today. Lyon, France: international agency for research on cancer, Available from: <https://gco.iarc.fr/today>. (Accessed 11 June 2019). <https://gco.iarc.fr/today> (accessed December 19, 2021).
- [7] H. Kang, X. Xiao, C. Huang, Y. Yuan, D. Tang, X. Dai, X. Zeng, Potent aromatase inhibitors and molecular mechanism of inhibitory action, *Eur. J. Med. Chem.* 143 (2018) 426–437, <https://doi.org/10.1016/j.ejmech.2017.11.057>.
- [8] G.T. Beatson, On the treatment of inoperable cases of carcinoma of the mamma: suggestions for a new method of treatment with illustrative cases, *Lancet* II (1896) 104–107, [https://doi.org/10.1016/S0140-6736\(01\)72384-7](https://doi.org/10.1016/S0140-6736(01)72384-7).

- [9] J. Caciolla, A. Spinello, S. Martini, A. Bisi, N. Zaffaroni, S. Gobbi, A. Magistrato, Targeting orthosteric and allosteric pockets of aromatase via dual-mode novel azole inhibitors, *ACS Med. Chem. Lett.* 11 (5) (2020) 732–739, <https://doi.org/10.1021/acsmchemlett.9b00591>.
- [10] F.B. De Abreu, G.N. Schwartz, W.A. Wells, G.J. Tsongalis, Personalized therapy for breast cancer, *Clin. Genet.* 86 (1) (2014) 62–67, <https://doi.org/10.1111/cge.12381>.
- [11] D. Ghosh, J. Lo, C. Egbuta, Recent progress in the discovery of next generation inhibitors of aromatase from the structure-function perspective, *J. Med. Chem.* 59 (11) (2016) 5131–5148, <https://doi.org/10.1021/acs.jmedchem.5b01281>.
- [12] S. Hiscox, E.L. Davies, P. Barrett-Lee, Aromatase inhibitors in breast cancer, *Maturitas* 63 (4) (2009) 275–279, <https://doi.org/10.1016/j.maturitas.2009.05.008>.
- [13] J.M. Dixon, Endocrine resistance in breast cancer, *New J. Sci.* 2014 (10) (2014) 1–27, <https://doi.org/10.1155/2014/390618>.
- [14] D. Ghosh, J. Griswold, M. Erman, W. Pangborn, Structural basis for androgen specificity and oestrogen synthesis in human aromatase, *Nature* 457 (7226) (2009) 219–223, <https://doi.org/10.1038/nature07614>.
- [15] A. Mojaddami, A. Sakhteman, M. Fereidoonhezad, Z. Faghih, A. Najdian, S. Khabnadideh, H. Sadeghpour, Z. Rezaei, Binding mode of triazole derivatives as aromatase inhibitors based on docking, protein ligand interaction fingerprinting, and molecular dynamics simulation studies, *Res. Pharm. Sci.* 12 (1) (2017) 21–30, <https://doi.org/10.4103/1735-5362.199043>.
- [16] W. Jessie, L. Zeruesenay, D.A. Flockhart, Tamoxifen metabolites as active inhibitors of aromatase in the treatment of breast cancer, *Breast Cancer Res. Treat.* 131 (2) (2012) 473–481, <https://doi.org/10.1007/s10549-011-1428-z>.
- [17] C. Egbuta, J. Lo, D. Ghosh, Mechanism of inhibition of estrogen biosynthesis by azole fungicides, 155, 2014, pp. 4622–4628, <https://doi.org/10.1210/en.2014-1561>. December.
- [18] A. Spinello, S. Martini, F. Berti, M. Pennati, M. Pavlin, J. Sgrignani, G. Grazioso, G. Colombo, N. Zaffaroni, A. Magistrato, European journal of medicinal Chemistry rational design of allosteric modulators of the aromatase enzyme : an unprecedented therapeutic strategy to fight breast cancer, *Eur. J. Med. Chem.* 168 (2019) 253–262, <https://doi.org/10.1016/j.ejmech.2019.02.045>.
- [19] A. Magistrato, J. Sgrignani, R. Krause, A. Cavalli, Single or Multiple access channels to the CYP450s active site? An answer from free energy simulations of the human aromatase enzyme, *J. Phys. Chem. Lett.* 8 (9) (2017) 2036–2042, <https://doi.org/10.1021/acs.jpclett.7b00697>.
- [20] J. Sgrignani, M. Bon, G. Colombo, A. Magistrato, Computational approaches elucidate the allosteric mechanism of human aromatase inhibition: a novel possible route to small-molecule regulation of CYP450s activities? *J. Chem. Inf. Model.* 54 (10) (2014) 2856–2868, <https://doi.org/10.1021/ci500425y>.
- [21] D. Ghosh, C. Egbuta, J. Lo, Testosterone complex and non-steroidal ligands of human aromatase, *J. Steroid Biochem. Mol. Biol.* 181 (2018) 11–19, <https://doi.org/10.1016/j.jsmb.2018.02.009>.
- [22] D. Ghosh, J. Lo, D. Morton, D. Valette, J. Xi, J. Griswold, S. Hubbell, C. Egbuta, W. Jiang, J. An, H.M.L. Davies, Novel aromatase inhibitors by structure-guided design, *J. Med. Chem.* 55 (19) (2012) 8464–8476, <https://doi.org/10.1021/jm300930n>.
- [23] M.R. Saberi, T.K. Vinh, S.W. Yee, B.J.N. Griffiths, P.J. Evans, C. Simons, Potent CYP19 (aromatase) 1-(Benzofuran-2-yl)(Phenylmethyl)Pyridine, -imidazole, and -triazole inhibitors: synthesis and biological evaluation, *J. Med. Chem.* 49 (3) (2006) 1016–1022, <https://doi.org/10.1021/jm0508282>.
- [24] S. Mahboobi, A. Sellmer, H. Höcher, C. Garhammer, H. Pongratz, T. Maier, T. Ciossek, T. Beckers, 2-Aroylindoles and 2-arylbzofurans with N-hydroxyacrylamide substructures as a novel series of rationally designed histone deacetylase inhibitors, *J. Med. Chem.* 50 (18) (2007) 4405–4418, <https://doi.org/10.1021/jm0703136>.
- [25] B. Schmidt, M. Riemer, U. Schilde, Chroman-4-ones via microwave-promoted domino claisen rearrangement-oxa-Michael addition: synthesis of tabchromones A and B, *Synlett* 25 (20) (2014) 2943–2946, 2014.
- [26] P.A. Foster, S.K. Chander, S.P. Newman, L.W.L. Woo, O.B. Sutcliffe, C. Bubert, D. Zhou, S. Chen, B.V.L. Potter, M.J. Reed, A. Purohit, A new therapeutic strategy against hormone-dependent breast cancer: the preclinical development of a dual aromatase and sulfatase inhibitor, *Clin. Cancer Res.* 14 (20) (2008) 6469–6477, <https://doi.org/10.1158/1078-0432.CCR-08-1027>.
- [27] Cyprotex Discovery Ltd, Cytochrome P450 (CYP) inhibition assay (IC₅₀). <https://www.cyprotex.com/admepk/in-vitro-metabolism/cytochrome-p450-inhibition/>, 29th November 2021.
- [28] Molecular Operating Environment (MOE) CCI, 2016, 1010 Sherbooke St. West, Suite #910, Montreal, QC, Canada, H3 A 2R7.
- [29] Schrödinger Release 2020-1: Desmond Molecular Dynamics System, D. E. Shaw Research, New York, NY, 2020. Maestro-Desmond Interoperability Tools, Schrödinger, New York, NY, 2020, <https://www.schrodinger.com/products/desmond>.
- [30] K.J. Bowers, E. Chow, H. Xu, R.O. Dror, M.P. Eastwood, B.A. Gregersen, J. L. Klepeis, I. Kolossvary, M.A. Moraes, F.D. Sacerdoti, K.K. Salmon, Y. Shan, D. E. Shaw, Scalable algorithms for molecular dynamics simulations on commodity clusters, in: Proceedings of the ACM/IEEE Conference on Supercomputing (SC06), Tampa, Florida, 2006, pp. 11–17. November, <https://dl.acm.org/doi/proceedings/10.1145/1188455>, 29th November 2021.
- [31] F.A.S. Binjubair, J.E. Parker, A.G. Warrilow, K. Puri, P.J. Braidley, E. Tatar, S. L. Kelly, D. Kelly, C. Simons, Small molecule inhibitors targeting 14 α -demethylase (CYP51): synthesis, molecular modeling and evaluation against *Candida albicans*, *ChemMedChem* 15 (2020) 1294–1309, <https://doi.org/10.1002/cmdc.202000250>.
- [32] N.A. Noureldin, J. Richards, H. Kothayer, M.M. Baraka, S.M. Eladl, W. Wootton, C. Simons, Design, computational studies, synthesis and *in vitro* antimicrobial evaluation of benzimidazole based thio-oxadiazole and thio-thiadiazole analogues, *BMC Chem.* 15 (1) (2021) 58, <https://doi.org/10.1186/s13065-021-00785-8>.